ACS APPLIED NANO MATERIALS

www.acsanm.org Article

Distinct Antibacterial Activities of Nanosized Cationic Liposomes against Gram-Negative Bacteria Correlate with Their Heterogeneous Fusion Interactions

Megan A. Laune,[†] Syed Ahad Zahidi,[†] Jared T. Wiemann,[†] and Yan Yu*

Cite This: *ACS Appl. Nano Mater.* 2022, 5, 15201−15210 Read Online

ACCESS | Metrics & More | Article Recommendations | Supporting Information

ABSTRACT: Nanosized liposomes are promising vehicles for delivering antibiotics to bacterial pathogens. Their fusion with bacterial membranes is hypothesized to enhance the potency of some antibiotics, but the mechanisms by which liposomes interact with bacteria are poorly understood. Liposome fusion with bacteria is typically detected using ensemble-averaged approaches based on the presumption that bacteria of the same species interact with liposomes homogeneously. Here, we challenge this presumption with observations of heterogeneous fusion interactions between cationic liposomes and the Gram-negative bacterium *Escherichia coli*. Importantly, the different interactions observed lead to different antibacterial outcomes. In one subpopulation, liposomes fused with both the outer and inner membranes of *E. coli*. In the second subpopulation, they fused only with the outer membrane. Liposomes caused permeabilization of the bacterial cell envelope and cell death only when they fuse with both the outer and inner membranes of *E. coli*. Compared to fusion, electrostatic binding of liposomes with the bacterial membrane has a significantly less effect in inhibiting bacterial growth. We further found that the fusion interactions of liposomes with bacteria vary across bacterial species. For the entire population of *Vibrio cholerae* studied, liposomes fused with only the outer membrane and thus had a negligible inhibitory effect. Our results demonstrate the significant level of heterogeneity in the interaction between nanomaterials and bacteria and highlight the consequent need to assess such interactions by mechanistic analysis at the level of the single cell.

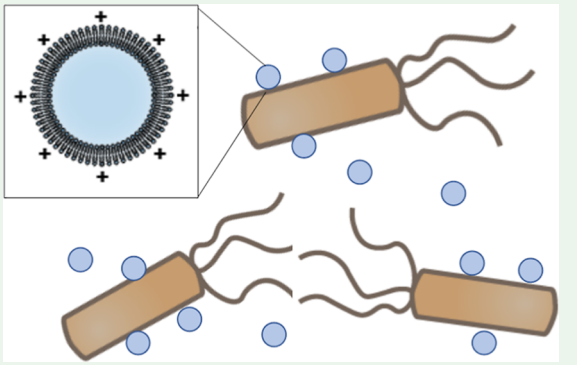

KEYWORDS: *liposome, antibacterial, Gram-negative bacteria, membrane fusion, heterogeneity*

INTRODUCTION

Liposomes are promising vehicles to deliver antibiotics. When antibiotics, like vancomycin, tobramycin, or polymyxin B, were encapsulated inside liposomes, they were found to inhibit bacterial growth at minimal concentrations that were 2−4 times lower than those needed for free antibiotics.[1−4] It is hypothesized that fusion of liposomes with the bacterial membrane contributes, at least partially, to this increase in potency. Cationic liposomes were shown to associate more strongly with both Gram-negative and Gram-positive bacteria.[5−8] Antibiotic-containing liposomes that were cationic were shown to exhibit higher potency than anionic liposomes in reducing cell viability in *Pseudomonas aeruginosa* and *Staphylococcus aureus* biofilms.[9] Further, cationic liposomes, such as those composed of dioctadecyldimethylammonium bromide (DODAB), even without an encapsulated antibiotic, have an inherent inhibitory effect against both Gram-negative and Gram-positive bacteria.[10−13] In a mechanistic study, the fusion of neutral liposomes with *Pseudomonasauregeinosa* was found to depend on several factors, including the cholesterol content of the liposomes, the content of phosphatidylethanolamine in the outer membrane of the bacteria, and divalent ions in the culture media.[3] Despite the insights provided by those studies, there has been no direct evidence to correlate liposome−bacterium fusion interaction with the antibacterial outcome. Additionally, studies on liposome−bacterium fusion were all done with ensemble-averaged measurements based on the presumption that liposomes interact with a particular species of bacteria in a homogeneous way. However, mounting evidence from biological studies does not support this presumption. The studies show that bacteria of the same genetic identity can form heterogeneous populations of phenotypic variants,[14−16] with heterogeneous cell-wall compositions and architectures.[17,18] How does this population heterogeneity of bacteria affect their interaction with liposomes?

Received: July 29, 2022
Accepted: October 3, 2022
Published: October 14, 2022

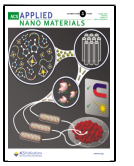

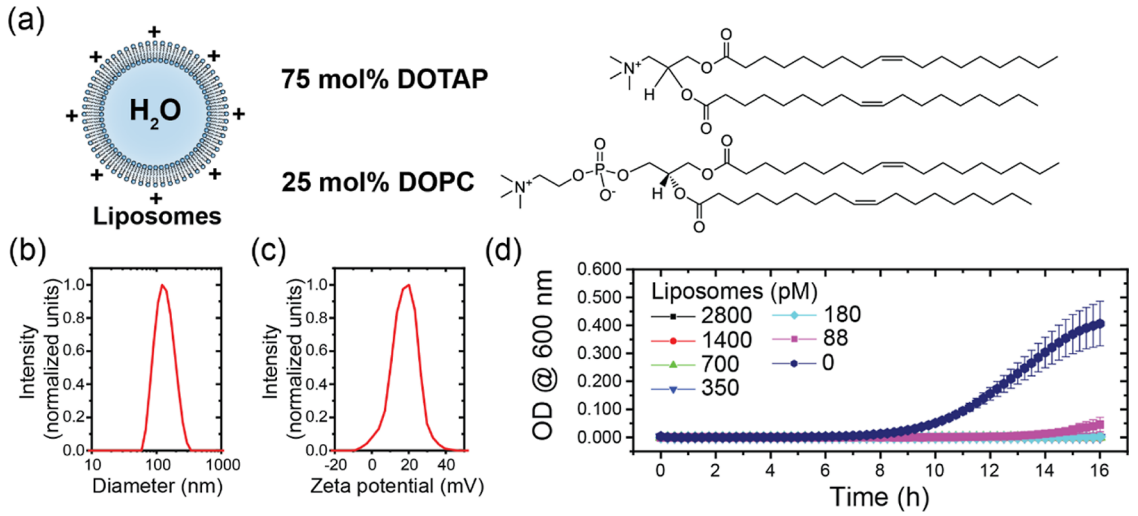

Figure 1. Antibacterial activity of liposomes against *E. coli*. (a) Schematic of the cationic liposomes, which were composed of 75:25 (mol/mol) DOTAP/DOPC. (b) Hydrodynamic diameter and (c) zeta potential of liposomes in 2 mM HEPES (pH 7.2). (d) Growth of *E. coli* in the presence of various concentrations of liposomes was measured as OD at 600 nm as a function of time. Each data point is the average of three samples collected on three different days. Error bars are standard error of the mean.

To address this question, in the current work, we investigated the fusion of cationic liposomes with Gram-negative bacteria by integrating single-cell quantitative imaging with ensemble-averaged antibacterial activity analysis. We found two subpopulations of *Escherichia coli* that exhibited different fusion interactions with liposomes. For one subpopulation, liposomes only fused with the outer membrane of the bacterium. In the other subpopulation, they fused with both the outer and inner membranes, leading to the permeabilization of the bacterial envelope and cell death. When liposomes fused with inner bacterial membranes, we found that their lipids propagated heterogeneously throughout the bacterial membrane. By comparing liposomes with bilayer-coated nanoparticles (NPs) having the same surface chemistry, we determined that liposome−bacterium fusion plays a more significant role than electrostatic attraction in driving the antibacterial potency of liposomes. Besides phenotypic heterogeneity within the same species of *E. coli*, we also found that the extent of fusion of cationic liposomes with Gram-negative bacteria, and consequently their antibacterial activity, varied across different bacterial species. Unlike the results for *E. coli*, we observed that cationic liposomes have less association with *Vibrio cholerae* than in the results for *E. coli*. Liposomes did not fuse with the bacterial inner membrane and had no inhibitory effect on the bacterial growth at concentrations of up to 2800 pM. The heterogeneity of these interactions between liposomes and bacteria may be a result of the intrinsic heterogeneity of bacterial cell surfaces even within the same group of genetically identical bacteria.

RESULTS AND DISCUSSION

Antibacterial Activity of Cationic Liposomes against *E. coli*. Liposomes used in this study were composed of 75 mol % 1,2-dioeleoyl-3-trimethylammonium-propane (DOTAP) and 25 mol % 1,2-dioeleoyl-*sn-glycero*-3-phosphatidylcholine (DOPC) (Figure 1a). DOTAP has a cationic head group and is expected to facilitate electrostatic attraction of liposomes to the highly negatively charged envelope of Gram-negative bacteria. The zwitterionic DOPC helps stabilize the curvature of the liposomes. After membrane extrusion preparation, the liposomes were monodisperse and approximately 100 nm in diameter, as confirmed using dynamic light scattering (DLS) (Figure 1b). The zeta potential of the liposomes was 24 ± 5 mV at pH 7.2, confirming their cationic charge (Figure 1c).

We first measured the inhibitory effect of cationic liposomes of various concentrations on the growth of *E. coli* over time (Figure 1d). A typical growth curve of *E. coli* in the absence of liposomes (0 pM) shows observable growth after about 8 h, resulting in an increase in the optical density (OD) of their growth medium at 600 nm wavelength (OD600). In the presence of an 88 pM concentration of liposomes, *E. coli* growth was delayed but not completely inhibited. However, with a 180 pM or higher concentration, observable bacterial growth was completely inhibited, as OD600 remained at the baseline for the entire measurement period of 18 h. Therefore, we determined that the minimal inhibitory concentration (MIC) of cationic liposomes against *E. coli* is 180 pM. This indicates the minimal concentration of liposomes needed to inhibit the growth of the entire bacterial culture, not the threshold concentration to kill all bacterial cells.

Liposome Fusion Enhances Antibacterial Activity. Previous studies have shown that many cationic NPs are effective against bacteria because they bind strongly to anionic bacterial membranes.[19−21] Cationic liposomes can also fuse with the outer membrane of bacteria. We asked whether the antibacterial activity of cationic liposomes against *E. coli* that we observed was driven by their electrostatic binding to the bacterial surface, by fusion with the bacterial membrane, or by the combination of both effects. To answer this question, we prepared bilayer-wrapped NPs by rupturing cationic liposomes on 100 nm silica NPs (particle schematic in Figure 2a). These bilayer-wrapped NPs had identical surface chemistry and size to the cationic liposomes studied. We confirmed this by measuring their zeta potential and hydrodynamic diameter, respectively (Figure S1). Given those similarities, the electrostatic attraction of the bilayer-wrapped NPs to the cell surface of the bacteria should have been the same as that for the liposomes. Unlike liposomes, however, they could not fuse with the bacterial outer membrane because of the strong adhesion force (electrostatic attraction and van der Waals

https://doi.org/10.1021/acsanm.2c03332
ACS Appl. Nano Mater. 2022, 5, 15201−15210

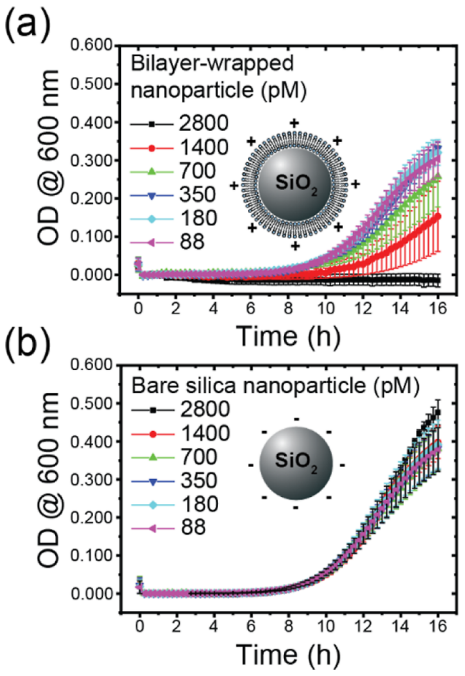

Figure 2. Antibacterial activity of bilayer-wrapped NPs against *E. coli*. Growth of *E. coli* in the presence of various concentrations of (a) bilayer-wrapped NPs and (b) bare silica NPs. Each data point is the average of three independent samples collected on different days. Error bars represent the standard error of the mean.

force) of a planar lipid bilayer on a negatively charged glass surface.[22] This was also later visualized and confirmed using fluorescence microscopy. We found that the concentration of the bilayer-wrapped NPs must be increased to 2800 pM to achieve the same inhibitory effect against *E. coli* as for 180 pM liposomes (Figure 2a). This demonstrates that the fusion of liposomes with the *E. coli* outer membrane is critical to their antibacterial activity. Electrostatic attraction also played a lesser additional role based on the comparison of results between lipid-wrapped NPs and bare silica NPs. Unlike lipid-wrapped NPs, bare silica NPs, which were negatively charged at pH 7.2, exhibited no inhibiting effect on *E. coli* growth even at 2800 pM (Figure 2b). This is consistent with the general recognition that anionic NPs typically are much less disruptive to bacteria than cationic NPs.[23−25]

Fusion Interaction of Liposomes with *E. coli*. To gain evidence that liposomes fuse with the outer membrane of *E. coli*, we first measured how the surface charge of *E. coli*, its zeta potential, changes after interaction with cationic liposomes. The zeta potential of *E. coli* that have not interacted with liposomes is highly negative (−47 ± 2 mV) (Figure 3a). This negative surface charge remained unchanged after interaction with 28 pM liposomes but increased drastically as the concentration of liposomes was increased to 280 pM and higher, reaching an average zeta potential of +9 ± 6 mV in the presence of 2800 pM liposomes. To further confirm that liposomes fused with the outer membrane of *E. coli* rather than simply being bound to its cell surface, we incubated *E. coli* with liposomes whose membranes contained 0.5 mol % Laurdan dye (Figure 3b). Laurdan is a solvatochromatic dye whose fluorescence emission peaks at around 490 nm wavelength in a disordered lipid phase but blue-shifts to 450 nm in a more ordered environment.[26] This peak shift is quantified as "generalized polarization"

$$\text{generalized polarization} = \frac{(I_{450} - I_{490})}{(I_{450} + I_{490})}$$

Changes in general polarization of Laurdan quantitatively indicate changes in membrane ordering.[27,28] After mixing the Laurdan-doped liposomes with *E. coli*, we observed a significant increase of 450 nm emission, causing the generalized polarization of Laurdan to increase from −0.30 ± 0.01 to −0.13 ± 0.04 (Figure 3c,d). This indicates that the lipid environment surrounding Laurdan becomes more

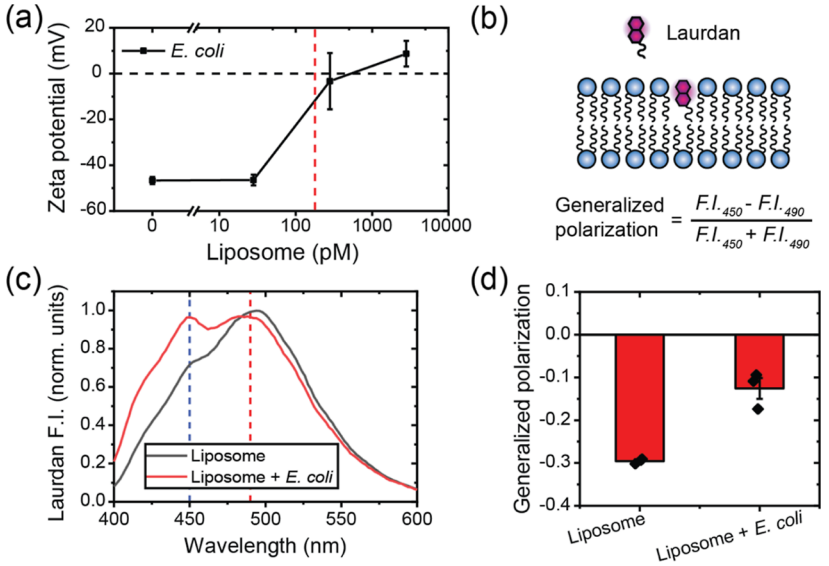

Figure 3. Liposomes fuse with *E. coli* membranes. (a) Zeta potential of *E. coli* after incubation with various concentrations of liposomes. The vertical, red dashed line indicates the MIC of liposomes against *E. coli* as determined in Figure 1. (b) Schematic of a lipid bilayer with a Laurdan dye inserted in the membrane and the equation for calculating generalized polarization. (c) Representative emission spectra of Laurdan in liposomes before and after incubation with *E. coli*. (d) Generalized polarization of Laurdan in liposomes before and after incubation with *E. coli*. Error bars in (a,d) are standard error of mean from three independent measurements performed on different days.

https://doi.org/10.1021/acsanm.2c03332
ACS Appl. Nano Mater. 2022, 5, 15201−15210

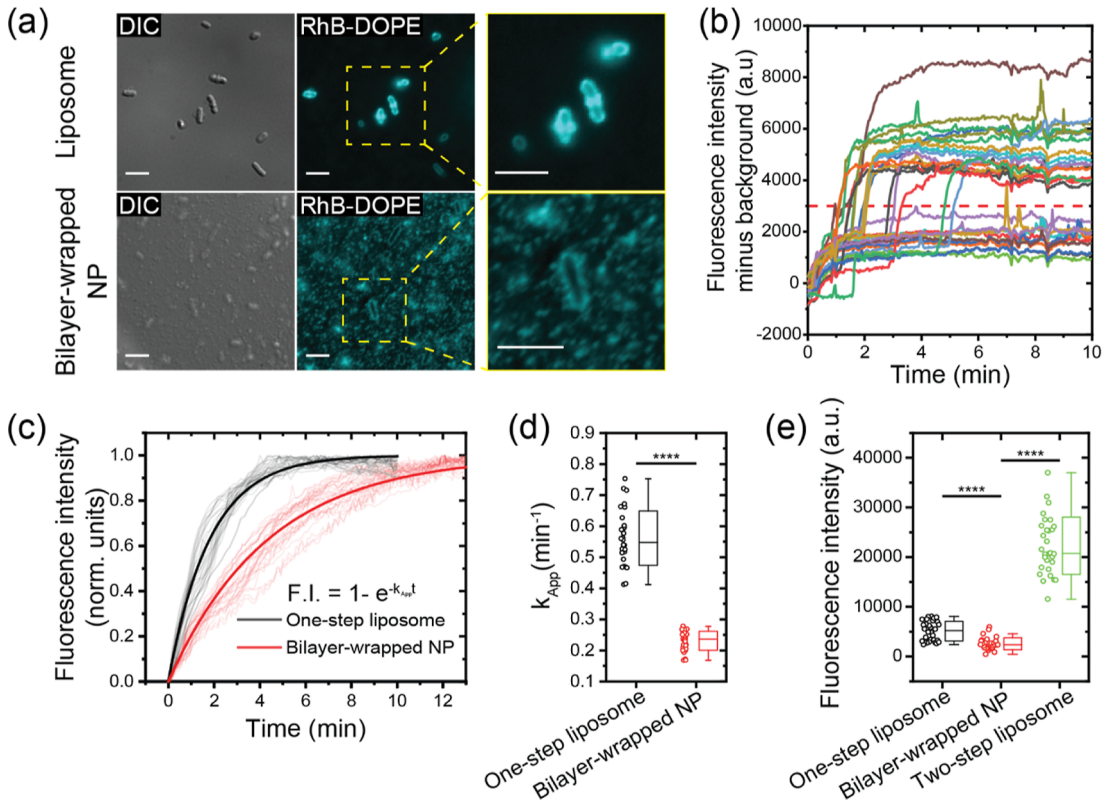

Figure 4. Fusion kinetics of liposomes with *E. coli*. (a) Epifluorescence and differential interference contrast images of *E. coli* (1×10^7 cfu/mL) after 10 min of incubation with 2800 pM liposomes (top) or bilayer-wrapped NPs (bottom) labeled with 0.2 mol % RhB-DOPE (cyan). Scale bars: 5 μm. (b) Fluorescence intensity of single *E. coli* as a function of time after fluorescent liposomes were added to the bacteria. Each curve represents data from a single bacterium. The dashed red line is shown to separate profiles of *E. coli* with one-step or two-step intensity increase. (n = 30 cells). (c) Quantification of *E. coli* fluorescence intensity as a function of time in the presence of fluorescent liposomes (2800 pM) or bilayer-wrapped NPs (2800 pM). Thin lines represent data of single bacteria (n = 30 cells for each group), all of which were normalized for the purpose of curve fitting. The thick solid lines are from fitting the average of each population with the equation shown in the inset. Only bacteria showing one-step intensity increase were included in this plot. (d) Apparent rate constants (k_{App}) obtained from fitting individual bacterial data in (c). (e) Steady-state fluorescence intensity of *E. coli* cells that exhibited one-step or two-step intensity increase in the presence of liposomes and *E. coli* cells in the presence of bilayer-wrapped NPs. Each boxplot in (d,e) indicates the maximum and minimum, the median (horizontal line), and the standard deviation of corresponding data. Statistical significance is noted by p values (from Student's t-test) as follows: ****$p < 0.0001$.

ordered after the liposome–*E. coli* interaction. This is consistent with our conclusion that liposomes fuse with the outer membrane of *E. coli*. After the fusion, Laurdan from liposomes are transferred into the bacterial membrane, which is known to be highly ordered by comparison to liposome membranes.[29]

Next, we imaged the fusion interactions of liposomes (2800 pM) with *E. coli*. Liposomes were made fluorescent by incorporating 0.2 mol % Rhodamine B (RhB)-DOPE (Figure 4a top) in their membrane. After 10 min of incubation, the *E. coli* cell surface became intensely and uniformly fluorescent, which confirms the transfer of the dye from liposomes to the bacterial outer membrane, and thus their fusion. Some bacteria formed large membrane blebs, likely due to having an excess of lipids in their outer membrane after it fused with liposomes (Figure S2). In contrast, for *E. coli* incubated with fluorescent lipid-wrapped NPs, the lipid-wrapped NPs can be seen as individual puncta bound to the bacterial cell surface (Figure 4a bottom). When analyzing images of *E. coli* after their interaction with fluorescent liposomes, we observed two populations of *E. coli* with drastically different levels of fluorescence intensities (Figure 4a top, more images in Figure S3). Upon addition of fluorescent liposomes to *E. coli*, the fluorescence intensity of all bacteria first increased at similar rates and plateaued within 1–2 min (Figure 4b, Movie S1). Afterward, about half of the bacterial population exhibited a second step of intensity increase. The starting time of the second step of intensity increase appeared stochastically, unlike the first step during which all bacteria exhibited fluorescence increases nearly simultaneously. This two-step intensity increase was only observed in *E. coli* that interacted with liposomes. When we performed a similar experiment using bilayer-wrapped NPs (2800 pM), we observed binding of the lipid-wrapped NPs, which appeared as puncta, to bacterial surfaces (Figure S4, Movie S2). By plotting the average fluorescence intensity of *E. coli* versus time and fitting the curves using the integrated rate equation for a one-step, reversible binding interaction, we found that the apparent rate constant, k_{App}, is significantly higher for *E. coli* interacted with liposomes ($k_{App} = 0.56 \pm 0.09$ min^{-1}) than those with bilayer-wrapped NPs ($k_{App} = 0.23 \pm 0.03$ min^{-1}) (Figure 4c,d). For direct comparison, only bacteria showing the one-step intensity increase were included in this analysis. Moreover, *E. coli* that interacted with liposomes reached an average fluorescence intensity of 5000 ± 2000 a.u. and 22,000 ± 6000 a.u after one-step and two-step intensity increase, respectively. In contrast, *E. coli* that interacted with bilayer-wrapped NPs reached an average fluorescence intensity of 3000 ± 1000 a.u (Figure 4e).

https://doi.org/10.1021/acsanm.2c03332
ACS Appl. Nano Mater. 2022, 5, 15201–15210

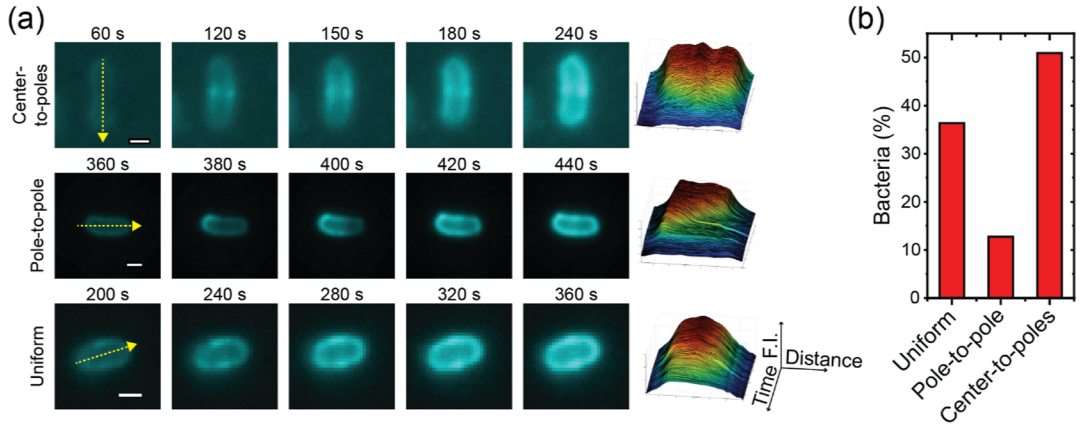

Figure 5. Propagation of fluorescence intensity. (a) Fluorescence images showing representative *E. coli* exhibiting different modes of fluorescence propagation during the two-step intensity increase. Surface plots show line-scan fluorescence intensity as a function of time. Scale bars: 1 μm. (b) Percentage of bacteria exhibiting each type of fluorescence propagation in the two-step intensity increase (n = 53 cells in total).

These observations indicate that fusogenic liposomes interact with *E. coli* more quickly and in greater numbers than do bilayer-wrapped NPs. Further, while analyzing fluorescence movies of cells which underwent the second step of liposome fusion, we found that the fluorescence intensity propagated across the cell envelope of single *E. coli* in several different ways during the second step of intensity increase (Figure 5a, videos of propagation in Movies S3–S5). The spread of fluorescence was seen to initiate from the center of a bacterium and propagate to its two poles (referred to as "center to pole") in ≈50% of *E. coli* cells. In ≈13% of cells, fluorescence appeared at one pole and propagated to the other pole ("pole to pole"). In ≈37% of cells, it started all over the cell envelope ("uniform") (Figure 5b). We next asked: what caused the two steps of intensity increase in a subpopulation of *E. coli* during their interaction with liposomes?

Propidium Iodide Assay. We hypothesized that liposomes first fuse with the outer membrane of all *E. coli* and then, in a subpopulation of cases, fuse with the inner membrane of *E. coli*. This would lead, in the first case, to a one-step intensity increase in the fluorescence of the bacterium and in the second case to a two-step increase. To test this hypothesis, we performed a propidium iodide (PI) imaging assay to detect cases where both layers of the bacterial membrane have been permeabilized. Propidium iodine is a membrane-impermeable dye that is weakly fluorescent in water but strongly fluorescent after intercalation with nucleic acids such as RNA and DNA. Staining of a bacterium by PI indicates that its cell envelope, including both the outer and inner membranes, has been permeabilized, thus allowing this dye to penetrate the cell and come into contact with its nucleic acids. Such permeabilization indicates that the cell is no longer viable. In experiments, we first incubated *E. coli* with 2800 pM liposomes (labeled with 0.2 mol % AF488-DOPE) for 1 h and then added 2 μM PI before fluorescence imaging (Figure 6a). We found that *E. coli* cells with stronger fluorescence of AF488-DOPE appeared to also have stronger fluorescence of PI.

To quantify this observation, we measured the PI and AF488-DOPE fluorescence intensities of single *E. coli* cells (N = 600) after their incubation with liposomes. The histogram of AF488-DOPE intensity shows two populations: ≈43% of cells with low intensity and ≈57% with high intensity. These correspond, respectively, to bacteria that had either one-step or two-step intensity increases (Figure 6b top). We then plotted the PI intensity of single bacteria as a function of their AF488-DOPE intensity (Figure 6b bottom). *E. coli* cells incubated with PI in the absence of liposomes (Figure S5) were used to determine the background level, indicated by the horizontal dashed line in Figure 5b. We determined that ≈38% of bacteria had PI intensities higher than the threshold, indicating that both the outer and inner membranes of those cells had been permeabilized. Importantly, nearly all those bacteria also had higher AF488-DOPE intensity, an indicator that they had undergone the two-step intensity increase after fusion with liposomes. In contrast, bacteria that underwent a one-step of intensity increase after liposome fusion, and therefore had low AF488-DOPE intensity, showed minimal permeabilization of their cell envelope. These data suggest that the two steps of intensity increase in *E. coli* after interaction with liposomes correspond to the liposome fusion with the bacterial outer and then inner membranes. When liposomes fuse with both membrane layers of *E. coli*, the interaction causes complete permeabilization of the cell envelope and the likely killing of the bacterium. When liposomes fuse with and permeabilize only the outer membrane, it does not cause cell death but could effectively inhibit cell growth. The two subpopulations of bacteria exhibiting different fusion interactions with liposomes were observed even at lower liposome concentrations, from 18 pM, 180 pM (MIC), to 1800 pM (Figure S6). However, the subpopulation of bacteria with both outer and inner membranes permeabilized increased significantly as liposome concentrations increased to 180 pM (MIC) and higher. We do not yet know the reason why lipids from liposome fusion propagate in bacterial membranes in three different ways, as shown in Figure 5. One possible explanation is that the *E. coli* cell envelope is intrinsically heterogeneous. There is some evidence for this heterogeneity. For example, cardiolipin, a negatively charged lipid, is known to concentrate at the poles and at the cell division septum of rod-shaped bacteria, including *E. coli*.[17,18] Areas of the membrane where such anionic lipids and proteins accumulate could serve as favorable sites for the binding and fusion of cationic liposomes.

Differential Impact of Liposomes against *V. cholerae*. To test whether our findings are specific to *E. coli* or generalizable to other Gram-negative bacteria, we investigated the interaction of cationic liposomes with *V. cholerae*, another common species of Gram-negative bacteria. First, we were

https://doi.org/10.1021/acsanm.2c03332
ACS Appl. Nano Mater. 2022, 5, 15201−15210

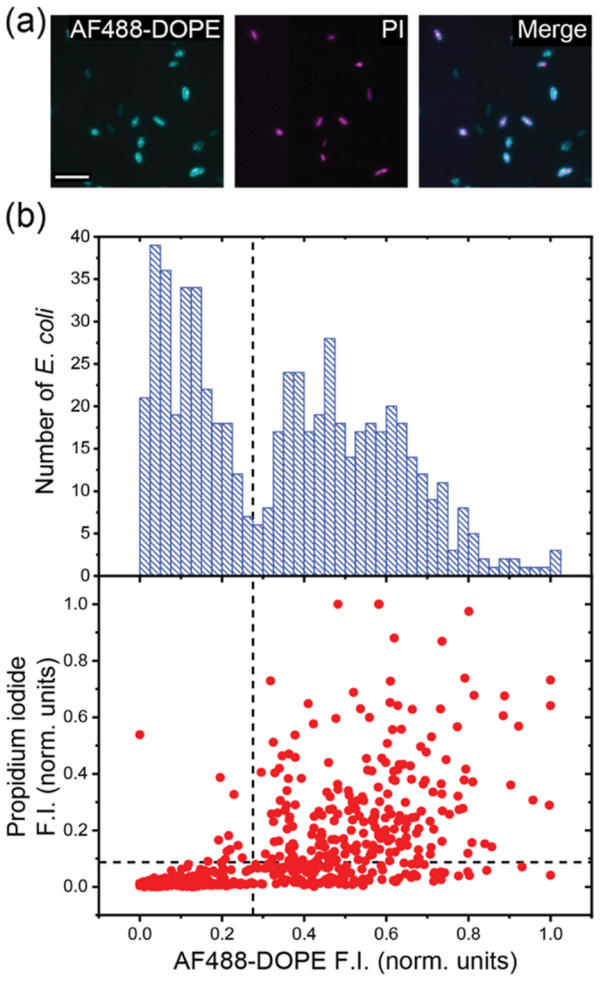

Figure 6. PI staining of *E. coli*. (a) Epifluorescence images of *E. coli* (1×10^7 cfu/mL) after 1 h of incubation with 2800 pM liposomes labeled with 0.2 mol % AF488-DOPE and 30 min incubation with 2 μM PI. Scale bar: 10 μm. (b) (top) Distribution of AF488-DOPE intensity of *E. coli* cells (n = 600) after incubation with liposomes. *E. coli* fluorescence intensity was determined from epifluorescence images. A vertical dashed line is used to distinguish two bacterial populations of different AF488-DOPE intensities. (Bottom) Scatter plot showing PI intensity and AF488-DOPE intensity of individual *E. coli* cells (n = 600) acquired from epifluorescence images. A horizontal dashed line indicates the threshold intensity of PI staining from control *E. coli* samples in the absence of liposomes.

surprised to find that neither liposomes nor bilayer-wrapped NPs inhibit *V. cholerae* at concentrations higher than 2800 pM (Figures 7 and S7). This is different from our results from *E. coli*. When we examined the interaction of *V. cholerae* with fluorescently labeled liposomes (Figure 8a), we only observed a one-step intensity increase (Figure 8b) This was unlike *E. coli* where, as described above, a subpopulation exhibited a two-step intensity increase. The steady-state fluorescence intensity of *V. cholerae* was slightly lower than the intensity of *E. coli* after a one-step intensity increase and significantly lower than the intensity of *E. coli* after a two-step intensity increase (Figure 8c). Because we confirmed that the step-wise intensity increase of *E. coli* resulted from liposome fusion with the outer and then with the inner membrane, these results indicate, first, that fewer liposomes bound to *V. cholerae* than to *E. coli* and, second, that liposomes only fused with the outer membrane of *V. cholerae* and not its inner membrane. The observed increase in zeta potential for *V. cholerae* due to fusion with liposomes was also significantly less than was observed for *E. coli*. This is despite the fact that both bacterial species have similarly strong negative charges (Figure 8d). This observation further supports the conclusion that liposomes are less likely to interact with *V. cholerae* than *E. coli*. Notably, the zeta potential of *V. cholerae* after interaction with 2800 pM liposomes did not shift to a positive zeta potential as in the case of *E. coli*. We further found that *V. cholerae* were very minimally stained with PI (Figure 8e, fluorescence images in Figure S8). This is evidence that the two layers of cell membranes surrounding these bacteria were never completely permeabilized after liposome fusion. This further confirms our conclusion that liposomes only fuse with the outer membrane of *V. cholerae*. The discrepancy of results between *E. coli* and *V. cholerae* demonstrates that cationic liposomes can interact differently with different species of Gram-negative bacteria. This difference in fusion interactions is likely resulted from the inherent heterogeneity in membrane composition and organization across different species of bacteria.[30,31] Importantly, the antibacterial potency of the cationic liposomes is determined by their mode of interaction. While *E. coli* and *V. cholerae* are only two representative species of the highly diverse Gram-negative bacteria, our findings suggest that the cationic liposomes are generally most potent against Gram-negative bacteria when they fuse with both outer and inner bacterial membranes.

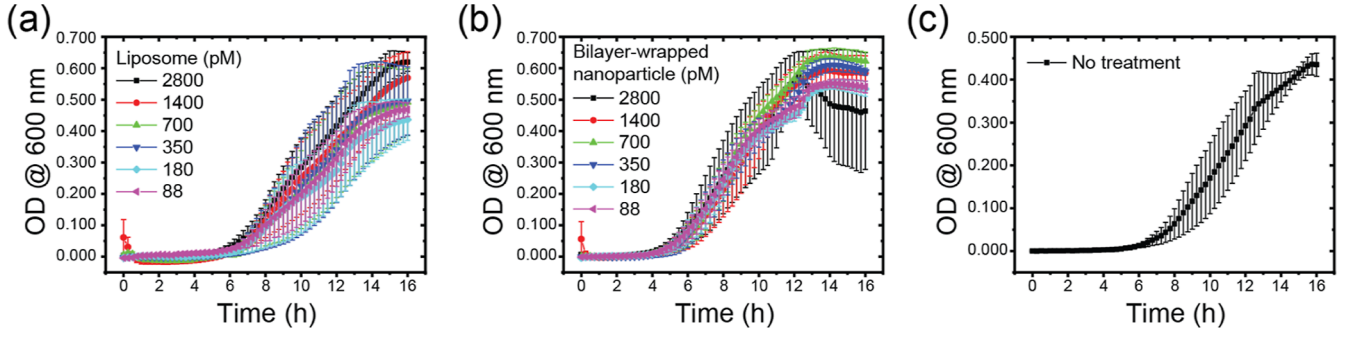

Figure 7. Antibacterial activities of (a) liposomes and (b) bilayer-wrapped NPs against *V. cholerae*. (c) Growth curve of *V. cholerae* without liposome interaction. Error bars are standard error of the mean from three independent measurements collected on different days.

https://doi.org/10.1021/acsanm.2c03332
ACS Appl. Nano Mater. 2022, 5, 15201−15210

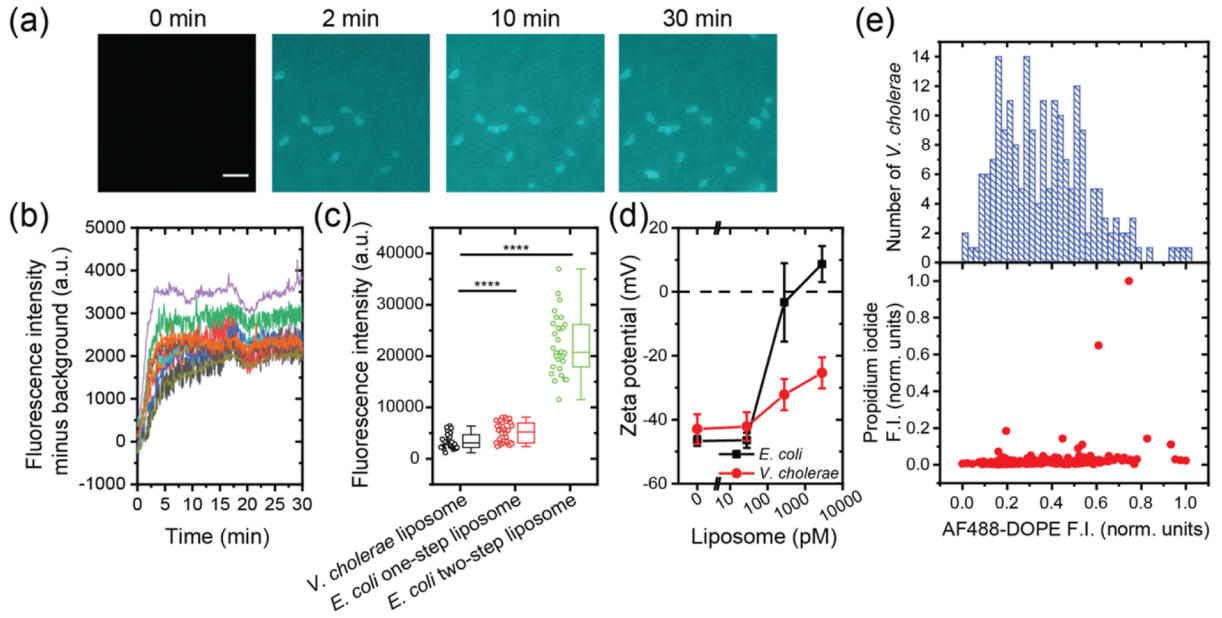

Figure 8. Characterization of liposome interactions with *V. cholerae* (a) Time series of epifluorescence images of *V. cholerae* (1×10^7 cfu/mL) incubated with 2800 pM fluorescently labeled liposomes (cyan). Scale bar: 10 μm. (b) Fluorescence intensity of individual bacteria as a function of time obtained from bacteria shown in (a). (c) Steady-state fluorescence intensity of bacteria cells after interaction with liposomes (n = 30 cells for each data group). Each boxplot indicates the maximum and minimum, the median (horizontal line), and the standard deviation of the corresponding data. Statistical significance is noted by p values (from Student's t-test) as follows: ****$p < 0.0001$. (d) Zeta potential of *V. cholerae* cells after incubation with lipid vesicles. *E. coli* data are included for comparison. (e) (Top) Distribution of AF488-DOPE intensity in single *V. cholerae* cells (n = 200) after incubation with liposomes. (Bottom) Scatter plot showing PI intensity and AF488-DOPE intensity of single *V. cholerae* cells (n = 200) acquired by epifluorescence microscopy. Cell intensity was determined from epifluorescence images.

CONCLUSIONS

Liposomes have been shown to fuse with some bacteria[5−8] and increase the permeability of the cell envelope of Gram-negative bacteria.[32] However, these fusion interactions have been studied only using ensemble-averaged approaches. This is based on the presumption that members of each bacterial species interact with liposomes in a homogeneous way. This study provides new grounds to question this presumption. We observed two different modes of fusion interaction of cationic liposomes with Gram-negative bacteria using *E. coli* and *V. cholerae* as two representative species. These two modes were observed even within a single species, and they led to different outcomes of anti-bacterial action. In the first mode of interaction, liposomes fused with only the outer membrane of a bacterium, even when a large excess of liposomes was available. This was observed for a sub-population of *E. coli* and for the entire population of *V. cholerae* tested. In the second mode of interaction, liposomes fuse with the bacterial outer membrane first and then with the inner membrane in two consecutive steps. This was observed in a second sub-population of *E. coli* but was never observed for *V. cholerae*. Even within this sub-population of *E. coli*, we saw a large variation in how lipids from liposomes propagate within the bacterial membrane after fusion. They propagated directionally from pole to pole, bi-directionally from cell mid-section to pole, or randomly over the entire membrane. This is an intriguing observation. It is unclear what molecular mechanisms contribute to or determine those different modes of lipid propagation. When liposomes fuse with both outer and inner membranes of *E. coli*, they readily permeabilize the bacterial cell envelope and cause cell death. The presence of the two sub-populations demonstrates that the two-step fusion of liposomes with the bacterial membranes is important for the bactericidal effect but not required for inhibiting bacterial growth. By comparison with the fusion of cationic liposomes with Gram-negative bacteria, the mere electrostatic attraction of liposomes to the bacteria was found to play a lesser but not negligible role in driving their anti-bacterial potency. We directly demonstrated this by comparing the antibacterial activity of cationic liposomes with that of silica NPs wrapped by a cationic lipid bilayer of the same composition. Silica NPs were electrostatically attracted to the bacteria, but their lipid bilayers could not undergo fusion with the bacterial membrane.

Our results demonstrate a significant level of heterogeneity in liposome interactions across different species of Gram-negative bacteria and even within members of the same species of bacteria. While cationic liposomes are potent in inhibiting the growth of *E. coli*, they had a negligible inhibitory effect on *V. cholerae*. The discrepancy is possibly because fewer liposomes bind to *V. cholerae*, and they only fuse with the outer membrane of these bacteria. This, however, may not be applicable to the effect of small-molecule antibiotics that could easily penetrate the inner bacterial membrane once the outer membrane is damaged. Within the same species of *E. coli*, liposomes fuse with and permeabilize bacterial membranes differently for different subpopulations of the bacteria. This results in drastically different potencies of liposomes for inhibiting bacterial growth. These observed differences are plausibly due to the intrinsic heterogeneity of bacterial cell surfaces, in both composition and architecture, within and between bacterial species.[17,18] For example, *V. cholerae* and *E. coli* have different peptidoglycan synthesis and turnover,[33] which directly impact how the bacterial cell walls respond and adapt to extracellular reagents such as the liposomes. Even different strains of *V. cholerae* or *E. coli* can have distinct structures of lipopolysaccharides.[34,35] Those cell wall differ-

https://doi.org/10.1021/acsanm.2c03332
ACS Appl. Nano Mater. 2022, 5, 15201−15210

ences can possibly contribute to the different responses of bacteria to the cationic liposomes. Our findings highlight this unexpected diversity, the consequent inadequacy of ensemble-averaged measurements as a sole means of characterizing antibacterial activities, and the need to complement such studies with mechanistic single-cell quantifications of the interactions of nanomaterials with bacteria.

MATERIALS AND METHODS

Cells and Reagents. *E. coli* (MG1655) was generously provided by Prof. J.P. Gerdt at Indiana University. Avirulent *V. cholerae* El Tor O1 strain was engineered and kindly gifted by Prof. A. Camilli at Tufts University. 1,2-Dioeleoyl-3-trimethylammonium-propane (DOTAP), 1,2-dioleoyl-*sn-glycero*-3-phosphocholine (DOPC), 1,2-dioleoyl-*sn-glycero*-3-phosphoethanolamine-*N*-(lissamine rhodamine B sulfonyl) (RhB-DOPE), and 1,2-dioleoyl-*sn-glycero*-3-phosphoethanolamine-*N*-(TopFluor AF488) (AF488-DOPE) were purchased from Avanti Polar Lipids, Inc. (Alabaster, AL, USA). Laurdan dye was purchased from Cayman Chemical Company, Inc. (Ann Arbor, MI, USA). Silica NPs (100 nm in diameter) were purchased from Nanocomposix (San Diego, CA, USA). Luria broth base and Luria−Bertani (LB) agar were purchased from Fisher Scientific (Waltham, MA, USA). M9 media was made using reagents from Sigma Aldrich (St. Louis, MO, USA). All media were sterilized using an autoclave or by filtration through a 0.22 μm diameter pore filter before use. Ultrapure water (18.2 MΩ cm) was used in all experiments.

Preparation and Characterization of Liposomes and Bilayer-Wrapped NPs. Cationic liposomes were made via extrusion. Briefly, lipid stock solution was made by mixing 75:25 DOTAP/DOPC (mol/mol) with a small amount of fluorescent lipid (0.2 mol % RhB-DOPE, 0.2 mol % AF488-DOPE, or 0.5 mol % Laurdan) in chloroform. The total lipid concentration in the stock solution was 5 mg/mL. The lipid stock solution was dried in a round-bottom flask under a gentle stream of nitrogen for 30 min. The resulting lipid film was then rehydrated using M9 minimal media to a total lipid concentration of 1 mg/mL under periodic vortexing at 40 °C for 1 h. The lipid suspension was then subjected to five freeze/thaw cycles. Liposomes were made by pushing the vesicle through a 100 nm polycarbonate membrane filter 11 times.

To make bilayer-wrapped NPs, 100 nm silica NPs were first suspended in M9 minimal media. Liposomes and silica NPs were mixed at a 2:1 (mol/mol) ratio, sonicated in a sonication bath for two min, and incubated in the dark at room temperature for 1 h. After incubation, bilayer-wrapped NPs were washed four times with M9 minimal media by using centrifugation (5 min at 14,000*g*) to remove excess liposomes. Bilayer-wrapped NPs were stored at 4 °C and used for up to 3 days after preparation. Hydrodynamic diameter and zeta potential of the liposomes and bilayer-wrapped NPs were measured using a Malvern Zetasizer (Indiana University Nanoscale Characterization Facility, Bloomington, IN). Liposome concentrations were calculated using fluorescence intensity measured by a BioTek H1 Synergy plate reader. Briefly, a calibration curve of fluorescence intensity as a function of lipid concentration was made by serial dilution of liposomes before extrusion. Lipid concentration (mg/mL) was measured after each sample preparation. Molar concentration of liposomes was calculated from mg/mL units assuming that each 100 nm liposome contains ∼97,000 lipid molecules based on the previous report that the molecular area of DOTAP in lipid bilayers is ∼65 Å^2/molecule.[36]

Bacteria Growth Conditions. Bacteria (*E. coli* or *V. cholerae*) were grown on LB agar plates overnight at 37 °C. Bacteria from each plate were inoculated into 5 mL of Luria broth in culture tubes and grown to a stationary phase at 37 °C with 280 rpm shaking. Bacteria were washed three times with 150 mM NaCl and then three times with M9 minimal media using centrifugation (2 min at 7000*g* each). Bacteria were then diluted to the desired concentration in M9 media and used immediately.

Measurement of MIC. MICs were determined using the standard broth microdilution technique[37] with slight modification. Bacteria (5 × 10^5 cfu/mL) were exposed to the desired concentrations of liposomes, bilayer-wrapped NPs, or bare silica NPs in M9 media in a 96-well plate. On each plate, a positive growth control consisting of bacteria and M9 minimal media and a negative growth control containing only M9 minimal media were included. Growth curves were obtained by measuring the OD at 600 nm every 15 min for 16 h at 37 °C using a BioTek H1 Synergy plate reader. To control for changes in the OD due to path length, we maintained a constant volume of 200 μL of solution in every plate reader measurement. Samples with NPs were performed in triplicate on each day. The MIC for each type of NP was determined as the lowest concentration at which no bacterial growth was observed after 16 h.

Fluorescence Imaging. Coverslips were cleaned by sonication in 70% EtOH and rinsed with ultrapure water. Epi-fluorescence and differential interference contrast (DIC) images were acquired using a Nikon Ti inverted microscope equipped with a 100×/1.49 NA TIRF objective. For each experiment, bacteria were mixed with the desired concentration of liposomes or bilayer-wrapped NPs to achieve 1 × 10^7 cfu/mL bacteria in M9 minimal media. Images were processed using ImageJ.

To analyze binding kinetics, the liposome−bacteria binding interaction was modeled based on a one-step, reversible binding interaction between liposomes (L) and bacterium (B)

$$B + L \underset{k_{off}}{\overset{k_{on}}{\rightleftharpoons}} BL$$

where BL is the liposome−bacterium complex, k_{on} is the association rate constant, and k_{off} is the dissociation rate constant. The apparent rate constant, k_{App}, was defined as

$$k_{App} = k_{on}[L] + k_{off}$$

where $[L]$ is constant because $L \gg B$ in the system. k_{app} was used to quantitatively compare kinetics of liposome and bilayer-wrapped NP binding to bacteria. To quantify fluorescence intensity of single cells as a function of time, the boundary of each cell was drawn manually in fluorescence microscopy images, and the mean fluorescence intensity for each cell in a given image was obtained. Only bacteria cells that were immobilized on the coverslip for the entirety of the imaging time were used for the kinetics measurements. The kinetics curves were first normalized between 0 and 1 and then fit to the following equation, as previously described,[38] to solve for k_{App}

$$\text{fluorescence intensity} = 1 - e^{(-k_{App}t)}$$

Fittings with $R^2 > 0.95$ were used for analysis.

Zeta Potential of Bacteria. Bacteria (*E. coli* or *V. cholerae*) were mixed with the desired concentration of liposomes in M9 media to reach a final bacteria concentration of 1 × 10^8 cfu/mL. Bacteria mixed with M9 media only were used as a control. Liposomes and bacteria were incubated for 30 min at 37 °C under 280 rpm shaking. After incubation, samples were washed six times with 2 mM HEPES (pH 7.2) using centrifugation (2 min at 7000*g*) to remove unbound liposomes. Zeta potential measurements of the bacteria were acquired using a Malvern Zetasizer Nano ZS (Nanoscale Characterization Facility at Indiana University).

PI Staining. Bacteria (*E. coli* or V. cholerae, 1 × 10^7 cfu/mL) and 2800 pM liposomes (labeled with 0.2 mol % AF488-DOPE) were incubated for 1 h in M9 minimal media at room temperature. After that, PI (final concentration 2 μM) was added to the bacteria/LUV mixture and incubated for 30 min at room temperature. Samples were immediately imaged using epi-fluorescence microscopy. The fluorescence intensity of single cells in the AF488-DOPE channel and PI channel was separately measured in ImageJ by manually drawing a boundary around each individual cell and measuring the mean pixel fluorescence intensity. To determine a fluorescence intensity threshold for PI influx, control samples without liposomes were prepared, and the PI intensity of each cell was measured (n = 200 bacteria). Cells with intensity greater than 3 standard deviations

https://doi.org/10.1021/acsanm.2c03332
ACS Appl. Nano Mater. 2022, 5, 15201−15210

above the mean intensity of the control sample were counted as those stained with PI.

Generalized Polarization of Laurdan. *E. coli* and 2800 pM liposomes (labeled with 0.5 mol % Laurdan) were incubated together for 30 min at room temperature. Excess liposomes were then washed away from *E. coli* by centrifugation (7000*g*, two min/wash, six total washes). Fluorescence emission of Laurdan at 450 and 490 nm at 360 nm excitation was measured using a BioTek Synergy H1 multi-mode microplate reader. Liposomes without bacteria were also measured as a control. Laurdan generalized polarization was calculated as follows

$$\text{generalized polarization} = \frac{(I_{450} - I_{490})}{(I_{450} + I_{490})}$$

where I_{450} and I_{490} are the emissions measured at 450 and 490 nm, respectively. Emission spectra were collected by exciting at 360 nm and measuring the fluorescence intensity from 400 to 600 nm in 2 nm steps.

■ ASSOCIATED CONTENT

Supporting Information

The Supporting Information is available free of charge at https://pubs.acs.org/doi/10.1021/acsanm.2c03332.

Fluorescence images of *E. coli* membrane blebbing; DLS and zeta potential results of liposome and bilayer-wrapped NPs; additional representative fluorescence and DIC images showing liposome−*E. coli* binding; fluorescence images showing bilayer-wrapped NPs binding to *E. coli*; additional representative fluorescence images of *E. coli* stained with PI in the presence and absence of liposomes; and fluorescence images of *V. cholerae* stained with PI in the presence of liposomes (PDF)

Liposomes binding to *E. coli* (AVI)

Binding of bilayer-wrapped NPs to *E. coli* (AVI)

Example of center-to-pole intensity propagation (AVI)

Example of pole-to-pole intensity propagation (AVI)

Example of uniform intensity propagation (AVI)

Liposome binding to *V. cholerae* (AVI)

■ AUTHOR INFORMATION

Corresponding Author

Yan Yu − *Department of Chemistry, Indiana University, Bloomington, Indiana 47405, United States;* orcid.org/0000-0001-6496-5045; Email: yy33@indiana.edu

Authors

Megan A. Laune − *Department of Chemistry, Indiana University, Bloomington, Indiana 47405, United States;* orcid.org/0000-0002-4361-2870

Syed Ahad Zahidi − *Department of Chemistry, Indiana University, Bloomington, Indiana 47405, United States*

Jared T. Wiemann − *Department of Chemistry, Indiana University, Bloomington, Indiana 47405, United States;* orcid.org/0000-0003-3416-0558

Complete contact information is available at: https://pubs.acs.org/10.1021/acsanm.2c03332

Author Contributions

†M.A.L., S.A.Z., and J.T.W. contributed equally to this work.

Notes

The authors declare no competing financial interest.

■ ACKNOWLEDGMENTS

We thank Prof. J.P. Gerdt at Indiana University and Prof. Andrew Camilli at Tufts University for providing bacterial cultures used in this study, and Dr. Yi Yi and Dr. Jun Chen at the Nanoscale Characterization Facility at Indiana University for assistance with instrument use. This work was supported by the National Science Foundation under grant no. 1705384 (expired before completion of this work) and no. 2153891. M.A.L. acknowledges the Undergraduate Summer Research Scholarship by the Department of Chemistry at Indiana University.

■ REFERENCES

(1) Nicolosi, D.; Scalia, M.; Nicolosi, V. M.; Pignatello, R. Encapsulation in fusogenic liposomes broadens the spectrum of action of vancomycin against Gram-negative bacteria. *Int. J. Antimicrob. Agents* **2010**, *35*, 553−558.

(2) Sachetelli, S.; Khalil, H.; Chen, T.; Beaulac, C.; Sénéchal, S.; Lagacé, J. Demonstration of a fusion mechanism between a fluid bactericidal liposomal formulation and bacterial cells. *Biochim. Biophys. Acta, Biomembr.* **2000**, *1463*, 254−266.

(3) Wang, Z.; Ma, Y.; Khalil, H.; Wang, R.; Lu, T.; Zhao, W.; Zhang, Y.; Chen, J.; Chen, T. Fusion between fluid liposomes and intact bacteria: study of driving parameters and in vitro bactericidal efficacy. *Int. J. Nanomed.* **2016**, *11*, 4025−4036.

(4) Omri, A.; Suntres, Z. E.; Shek, P. N. Enhanced activity of liposomal polymyxin B against Pseudomonas aeruginosa in a rat model of lung infection. *Biochem. Pharmacol.* **2002**, *64*, 1407−1413.

(5) Ibaraki, H.; Kanazawa, T.; Chien, W.-Y.; Nakaminami, H.; Aoki, M.; Ozawa, K.; Kaneko, H.; Takashima, Y.; Noguchi, N.; Seta, Y. The effects of surface properties of liposomes on their activity against Pseudomonas aeruginosa PAO-1 biofilm. *J. Drug Deliv. Sci. Technol.* **2020**, *57*, 101754.

(6) Wang, Y. Liposome as a delivery system for the treatment of biofilm-mediated infections. *J. Appl. Microbiol.* **2021**, *131*, 2626−2639.

(7) Rukavina, Z.; Vanić, Ž. Current Trends in Development of Liposomes for Targeting Bacterial Biofilms. *Pharmaceutics* **2016**, *8*, 18.

(8) Drulis-Kawa, Z.; Gubernator, J.; Dorotkiewicz-Jach, A.; Doroszkiewicz, W.; Kozubek, A. A comparison of the in vitro antimicrobial activity of liposomes containing meropenem and gentamicin. *Cell. Mol. Biol. Lett.* **2006**, *11*, 360−375.

(9) Dong, D.; Thomas, N.; Thierry, B.; Vreugde, S.; Prestidge, C. A.; Wormald, P.-J. Distribution and Inhibition of Liposomes on Staphylococcus aureus and Pseudomonas aeruginosa Biofilm. *PLoS One* **2015**, *10*, No. e0131806.

(10) Campanhã, M. T. N.; Mamizuka, E. M.; Carmona-Ribeiro, A. M. Interactions between cationic liposomes and bacteria: the physical-chemistry of the bactericidal action. *J. Lipid Res.* **1999**, *40*, 1495−1500.

(11) Martins, L. M. S.; Mamizuka, E. M.; Carmona-Ribeiro, A. M. Cationic Vesicles as Bactericides. *Langmuir* **1997**, *13*, 5583−5587.

(12) Tapias, G. N.; Sicchierolli, S. M.; Mamizuka, E. M.; Carmona-Ribeiro, A. M. Interactions between Cationic Vesicles and Escherichia coli. *Langmuir* **1994**, *10*, 3461−3465.

(13) Sicchierolli, S. M.; Mamizuka, E. M.; Carmona-Ribeiro, A. M. Bacteria Flocculation and Death by Cationic Vesicles. *Langmuir* **1995**, *11*, 2991−2995.

(14) Bruhn-Olszewska, B.; Szczepaniak, P.; Matuszewska, E.; Kuczyńska-Wiśnik, D.; Stojowska-Swędrzyńska, K.; Moruno Algara, M.; Laskowska, E. Physiologically distinct subpopulations formed in Escherichia coli cultures in response to heat shock. *Microbiol. Res.* **2018**, *209*, 33−42.

(15) Taniguchi, Y.; Choi, J.; Li, G.-W.; Chen, H.; Babu, M.; Hearn, J.; Emili, A.; Xie, X. S. Quantifying E. coli Proteome and Transcriptome with Single-Molecule Sensitivity in Single Cells. *Science* **2010**, *329*, 533−538.

(16) Ackermann, M. A functional perspective on phenotypic heterogeneity in microorganisms. *Nat. Rev. Microbiol.* **2015**, *13*, 497−508.
(17) Renner, D.; Weibel, B. Cardiolipin microdomains localize to negatively curved regions of Escherichia coli membranes. *Proc. Natl. Acad. Sci. U.S.A.* **2011**, *108*, 6264−6269.
(18) Kawai, F.; Shoda, M.; Harashima, R.; Sadaie, Y.; Hara, H.; Matsumoto, K. Cardiolipin Domains in Bacillus subtilis Marburg Membranes. *J. Bacteriol.* **2004**, *186*, 1475−1483.
(19) Feng, Z. V.; Gunsolus, I. L.; Qiu, T. A.; Hurley, K. R.; Nyberg, L. H.; Frew, H.; Johnson, K. P.; Vartanian, A. M.; Jacob, L. M.; Lohse, S. E.; Torelli, M. D.; Hamers, R. J.; Murphy, C. J.; Haynes, C. L. Impacts of gold nanoparticle charge and ligand type on surface binding and toxicity to Gram-negative and Gram-positive bacteria. *Chem. Sci.* **2015**, *6*, 5186−5196.
(20) Jacobson, K. H.; Gunsolus, I. L.; Kuech, T. R.; Troiano, J. M.; Melby, E. S.; Lohse, S. E.; Hu, D.; Chrisler, W. B.; Murphy, C. J.; Orr, G.; Geiger, F. M.; Haynes, C. L.; Pedersen, J. A. Lipopolysaccharide Density and Structure Govern the Extent and Distance of Nanoparticle Interaction with Actual and Model Bacterial Outer Membranes. *Environ. Sci. Technol.* **2015**, *49*, 10642−10650.
(21) Gupta, A.; Landis, R. F.; Li, C.-H.; Schnurr, M.; Das, R.; Lee, Y.-W.; Yazdani, M.; Liu, Y.; Kozlova, A.; Rotello, V. M. Engineered Polymer Nanoparticles with Unprecedented Antimicrobial Efficacy and Therapeutic Indices against Multidrug-Resistant Bacteria and Biofilms. *J. Am. Chem. Soc.* **2018**, *140*, 12137−12143.
(22) Orozco-Alcaraz, R.; Kuhl, T. L. Interaction Forces between DPPC Bilayers on Glass. *Langmuir* **2013**, *29*, 337−343.
(23) El Badawy, A. M.; Silva, R. G.; Morris, B.; Scheckel, K. G.; Suidan, M. T.; Tolaymat, T. M. Surface Charge-Dependent Toxicity of Silver Nanoparticles. *Environ. Sci. Technol.* **2011**, *45*, 283−287.
(24) Zhao, Y.; Tian, Y.; Cui, Y.; Liu, W.; Ma, W.; Jiang, X. Small Molecule-Capped Gold Nanoparticles as Potent Antibacterial Agents That Target Gram-Negative Bacteria. *J. Am. Chem. Soc.* **2010**, *132*, 12349−12356.
(25) Arakha, M.; Pal, S.; Samantarrai, D.; Panigrahi, T. K.; Mallick, B. C.; Pramanik, K.; Mallick, B.; Jha, S. Antimicrobial activity of iron oxide nanoparticle upon modulation of nanoparticle-bacteria interface. *Sci. Rep.* **2015**, *5*, 14813.
(26) Gunther, G.; Malacrida, L.; Jameson, D. M.; Gratton, E.; Sánchez, S. A. LAURDAN since Weber: The Quest for Visualizing Membrane Heterogeneity. *Acc. Chem. Res.* **2021**, *54*, 976−987.
(27) Kaiser, H.-J.; Lingwood, D.; Levental, I.; Sampaio, J. L.; Kalvodova, L.; Rajendran, L.; Simons, K. Order of lipid phases in model and plasma membranes. *Proc. Natl. Acad. Sci. U.S.A.* **2009**, *106*, 16645−16650.
(28) Parasassi, T.; De Stasio, G.; d'Ubaldo, A.; Gratton, E. Phase fluctuation in phospholipid membranes revealed by Laurdan fluorescence. *Biophys. J.* **1990**, *57*, 1179−1186.
(29) Nikaido, H. Molecular Basis of Bacterial Outer Membrane Permeability Revisited. *Microbiol. Mol. Biol. Rev.* **2003**, *67*, 593.
(30) Weihs, F.; Wacnik, K.; Turner, R. D.; Culley, S.; Henriques, R.; Foster, S. J. Heterogeneous localisation of membrane proteins in Staphylococcus aureus. *Sci. Rep.* **2018**, *8*, 3657.
(31) Vissers, T.; Brown, A. T.; Koumakis, N.; Dawson, A.; Hermes, M.; Schwarz-Linek, J.; Schofield, A. B.; French, J. M.; Koutsos, V.; Arlt, J.; Martinez, V. A.; Poon, W. C. K. Bacteria as living patchy colloids: Phenotypic heterogeneity in surface adhesion. *Sci. Adv.* **2018**, *4*, No. eaao1170.
(32) Moreira, L.; et al. Liposome Delivery of Nucleic Acids in Bacteria: Toward In Vivo Labeling of Human Microbiota. *ACS Infect. Dis.* **2022**, *8*, 1218−1230.
(33) Alvarez, L.; Hernandez, S. B.; Cava, F. Cell Wall Biology of Vibrio cholerae. *Annu. Rev. Microbiol.* **2021**, *75*, 151−174.
(34) Chatterjee, S. N.; Chaudhuri, K. Lipopolysaccharides of Vibrio cholerae: I. Physical and chemical characterization. *Biochim. Biophys. Acta, Mol. Basis Dis.* **2003**, *1639*, 65−79.
(35) Hase, S.; Rietschel, E. T. Isolation and Analysis of the Lipid A Backbone. Lipid A Structure of Lipopolysaccharides from Various Bacterial Groups. *Eur. J. Biochem.* **1976**, *63*, 101−107.
(36) Zhao, W.; Gurtovenko, A. A.; Vattulainen, I.; Karttunen, M. Cationic Dimyristoylphosphatidylcholine and Dioleoyloxytrimethylammonium Propane Lipid Bilayers: Atomistic Insight for Structure and Dynamics. *J. Phys. Chem. B* **2012**, *116*, 269−276.
(37) Wiegand, I.; Hilpert, K.; Hancock, R. E. W. Agar and broth dilution methods to determine the minimal inhibitory concentration (MIC) of antimicrobial substances. *Nat. Protoc.* **2008**, *3*, 163−175.
(38) Wheaten, S. A.; Ablan, F. D. O.; Spaller, B. L.; Trieu, J. M.; Almeida, P. F. Translocation of Cationic Amphipathic Peptides across the Membranes of Pure Phospholipid Giant Vesicles. *J. Am. Chem. Soc.* **2013**, *135*, 16517−16525.

https://doi.org/10.1021/acsanm.2c03332
ACS Appl. Nano Mater. 2022, 5, 15201−15210